Wind Turbine Control Based on Computational Fluid Dynamics (CFD) and Its Economic Effects

Takanori Uchida [1]

[1] Research Institute for Applied Mechanics Kyushu University, Kasuga, 816-8580; E-Mail: takanori@riam.kyushu-u.ac.jp (T.U.)

* Author to whom correspondence should be addressed; E-Mail: takanori@ riam.kyushu-u.ac.jp; Tel.: +81-92-583-7776; Fax: +81-92-583-7779.

Abstract: At the Atsumi Wind Farm in Aichi Prefecture, Japan, damage to wind turbines occurred frequently due to terrain-induced turbulence. In the present study, numerical analyses of terrain-induced turbulence were conducted by reproducing the topography in the vicinity of the wind turbine sites in high resolution and using RIAM-COMPACT natural terrain version, which is based on large eddy simulation (LES). The results of the diagnoses indicated that, in the case of south-easterly wind, terrain-induced turbulence is generated at a small terrain feature located upstream of Wind Turbine (WT) #2, which serves as the origin of the turbulence. At the Atsumi Wind Farm, a combination of the series of wind diagnoses and on-site operation experience led to a decision to adopt an "automatic shutdown program" for WTs #1 and #2. Here, "automatic shutdown program" refers to the automatic suspension of wind turbine operation upon the wind speed and direction meeting the conditions associated with significant effects of terrain-induced turbulence at a wind turbine site. The adoption of the "automatic shutdown program" has successfully resulted in a large reduction in the number of occurrences of wind turbine damage, thus, creating major positive economic effects. 1) a reduction in the repair costs by 9.322 million yen per year per wind turbine, 2) an increase in the availability factor by 8.05%, and 3) an increase in the capacity factor by 1.7%.

Keywords: complex terrain; CFD; terrain-induced turbulence; economic effects

1. Introduction

Recently, the wind power industry has undergone rapid growth at an unprecedented rate across the world. This growth has been occurring because wind power generation has the best cost performance of all the renewable energies in terms of achieving a post-fossil fuel society and reducing CO_2 emissions. There is no doubt that wind power is the leading renewable energy even in Japan. The authors are convinced that further dissemination of wind power generation will contribute on the global scale to "green innovation," efforts to combat global warming.

One technical issue which needs to be resolved in the near future in the field of wind power generation is to establish a numerical wind synopsis prediction technique which allows 1) accurate assessment of the local wind synopsis for wind turbines and 2) identification of local wind risks (terrain-induced turbulence) to wind turbines [1-8].

The numerical wind synopsis prediction technique RIAM-COMPACT (Research Institute for Applied Mechanics, Kyushu University, COMputational Prediction of Airflow over Complex Terrain), which has been developed by authors' research group, has a potential to resolve the above-mentioned issue all at once [9-16]. The core technology of RIAM-COMPACT is under continuous development at the Research Institute for Applied Mechanics, Kyushu University.

Recently, it has been reported that the availability factors of wind turbines on wind farms situated on complex terrain fall short of those originally projected; that is, reports of damage and breakage of the exteriors and interiors of wind turbines (e.g., breakage of yaw motors and yaw gears and cracks on wind turbine blades) as well as wind turbines with notably low power output have surfaced. The main cause of these problems is that small variations in the topographical relief in the vicinity of wind turbines serve as the origin of turbulence (terrain-induced turbulence). The present paper will discuss a specific example of a wind-risk (terrain-induced turbulence) diagnosis using the RIAM-COMPACT natural terrain version software.

2. Summary of the RIAM-COMPACT Natural Terrain Version Software

In the present study, the RIAM-COMPACT natural terrain version software [9-16] is used to numerically predict airflows over complex terrain with high accuracy while avoiding numerical instability. The RIAM-COMPACT natural terrain version software uses collocated grids in a general curvilinear coordinate system. In these collocated grids, the velocity components and pressure are defined at the cell centers, and variables which result from the contravariant velocity components multiplied by the Jacobian are defined at the cell faces. As for the simulation technique, the finite-difference method (FDM) is adopted, and a Large-Eddy Simulation (LES) model is used for the turbulence model. In LES, a spatial filter is applied to the flow field to separate eddies of various scales into grid scale (GS) components, which are larger than the computational grid cells, and subgrid scale (SGS) components, which are smaller than the computational grid cells. Large-scale eddies, i.e., the GS components of turbulence eddies, are directly numerically simulated without relying on the use of a physically simplified model. On the other hand, the main effect of small-scale eddies, i.e., the SGS components, is to dissipate energy, and this dissipation is modeled based on the physical considerations of the SGS stress.

For the governing equations of the flow, a spatially-filtered continuity equation for incompressible fluid (Eq. (1)) and a spatially filtered Navier-Stokes equation (Eq. (2)) are used:

$$\frac{\partial \overline{u}_i}{\partial x_i} = 0 \qquad -(1)$$

$$\frac{\partial \overline{u}_i}{\partial t} + \overline{u}_j \frac{\partial \overline{u}_i}{\partial x_j} = -\frac{\partial \overline{p}}{\partial x_i} + \frac{1}{Re}\frac{\partial^2 \overline{u}_i}{\partial x_j \partial x_j} - \frac{\partial \tau_{ij}}{\partial x_j} \qquad -(2)$$

Supporting equations are given in Eqs. (3) - (8):

$$\tau_{ij} \approx \overline{u'_i u'_j} \approx \frac{1}{3}\overline{u'_k u'_k}\delta_{ij} - 2\nu_{SGS}\overline{S}_{ij} \qquad -(3)$$

$$\nu_{SGS} = \left(C_s f_s \Delta\right)^2 \left|\overline{S}\right| \qquad -(4)$$

$$\left|\overline{S}\right| = \left(2\overline{S}_{ij}\overline{S}_{ij}\right)^{1/2} \qquad -(5)$$

$$\overline{S}_{ij} = \frac{1}{2}\left(\frac{\partial \overline{u}_i}{\partial x_j} + \frac{\partial \overline{u}_j}{\partial x_i} \right) \qquad \text{-(6)}$$

$$f_s = 1 - exp\left(-z^+ / 25\right) \qquad \text{-(7)}$$

$$\Delta = \left(h_x h_y h_z\right)^{1/3} \qquad \text{-(8)}$$

Because mean wind speeds of 6 m/s or higher are considered in the present study, the effect of vertical thermal stratification (density stratification), which is generally present in the atmosphere, is neglected. Furthermore, the effect of surface roughness is included by reconstructing the irregularities of the terrain surface in high resolution.

The computational algorithm and the time marching method are based on a fractional-step (FS) method [17] and the Euler explicit method, respectively. The Poisson's equation for pressure is solved by the successive over-relaxation (SOR) method. For discretization of all the spatial terms in Eq. (2) except for the convective term, a second-order central difference scheme is applied. For the convective term, a third-order upwind difference scheme is applied. An interpolation technique based on four-point differencing and four-point interpolation by Kajishima [18] is used for the fourth-order central differencing that appears in the discretized form of the convective term. For the weighting of the numerical diffusion term in the convective term discretized by third-order upwind differencing, $\alpha = 3$ is commonly applied in the Kawamura-Kuwahara Scheme [19]. However, $\alpha = 0.5$ is used in the present study to minimize the influence of numerical diffusion. For LES subgrid-scale modeling, the commonly used Smagorinsky model [20] is adopted. A wall-damping function is used with a model coefficient of 0.1.

3. Wind Synopsis Analysis with the RIAM-COMPACT Natural Terrain Version Software

As described earlier, the availability factors of wind turbines in wind farms on complex terrain often fall below the originally projected values. In other words, problems such as wind turbines with notably low power output and damage and breakage of the exteriors and interiors of wind turbines have surfaced. The effects of turbulence (terrain-induced turbulence) have also been made note of for the Atsumi Wind Farm in Aichi Prefecture, Japan, the site investigated in the present study. In the present paper, an LES turbulence simulation is conducted in high resolution using the RIAM-COMPACT natural terrain version software. The main purpose of this simulation is to reproduce the actual wind conditions at the wind farm in a visualized form.

3.1. Summary of the Atsumi wind farm

A wind synopsis analysis was performed for the Atsumi Wind Farm (in operation since March 2007) with the cooperation of Kyudenko Corporation (see Figs. 1, 2, and 3 and Table 1).

Figure 1. Terrain at and in the vicinity of the Atsumi wind farm, Aichi Prefecture, Japan (Source: Google Earth)


Figure 2. A photo of the wind turbine site (taken by one of the authors from the north-west). Note: Minor landforms of 125 m in elevation can be seen behind WT2 (Wind Turbine 2).

Table 1. Summary of the Atsumi wind farm

	WT1 to WT4
Wind turbine manufacturer, output	Vestas Wind Systems A/S V80-2.0 MW
Wind turbine height (ground surface to hub center height)	78m
Blade diameter	80m

**Figure 3.** A photo of WT1 showing specifications of the wind turbines
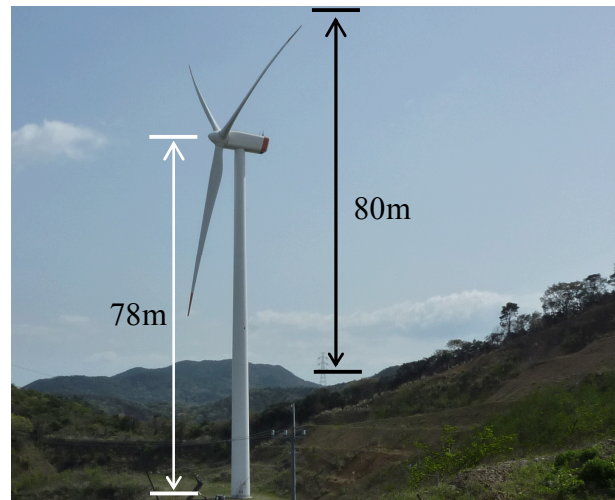
3.2. Simulation set-up

As shown in Fig. 4, the dimensions of the computational domain are 3.5 (x) × 1.5 (y) × 0.6 (z) km, where x, y, and z are the streamwise, spanwise, and vertical directions, respectively.

The terrain elevation data[12] were created with a spatial resolution of 5 m using contour lines from the basis map information of the Geospatial Information Authority of Japan (map scale 1 : 25000).

The numbers of computational grid points are 201 × 151 × 41 in the x-, y-, and z-directions, respectively, totaling approximately 1.24 million grid points. The grid spacing in the x- and y-directions is set unevenly so that the distribution of grid cells is characterized by high density in the vicinity of the wind turbines. Similarly, the grid spacing in the z-direction is set unevenly so that the density of grid cells increases smoothly toward the ground surface. The minimum horizontal and vertical grid spacings are 3 m and 0.6 m, respectively.

The wind direction set in the present simulation is south-easterly, which is a wind direction associated with confirmed abnormalities of wind turbines at this site. The wind velocity profile applied at the inflow boundary is that for surface roughness classification III (Fig. 6). Furthermore, slip conditions are applied at the side and upper boundaries and convective outflow conditions are applied at the outflow boundary. At the ground surface, non-slip boundary conditions are applied. The non-dimensional parameter Re in Eq. (2) is the Reynolds number ($=U_{in}h/\nu$) and is set to 10^4 [13]. Fig. 7 illustrates the characteristic scales relevant in the present simulation: h is the difference between the minimum and maximum ground surface elevations within the computational domain, U_{in} is the wind velocity at the inflow boundary at the height of the maximum ground surface elevation within the computational domain, and ν is the coefficient of dynamic viscosity of air. The time step is set to $\Delta t = 2 \times 10^{-3}\, h/U_{in}$.
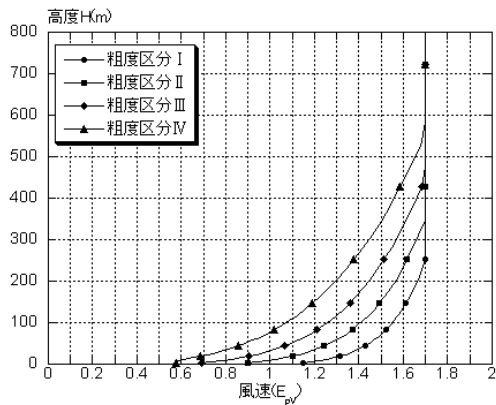
Figure 4. Computational domain, bird's eye view, colors indicate the elevation (maximum: 130m, minimum: 10m)
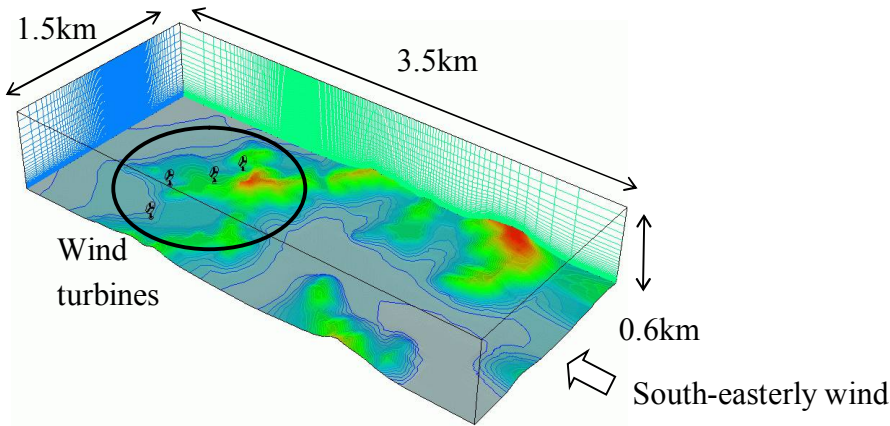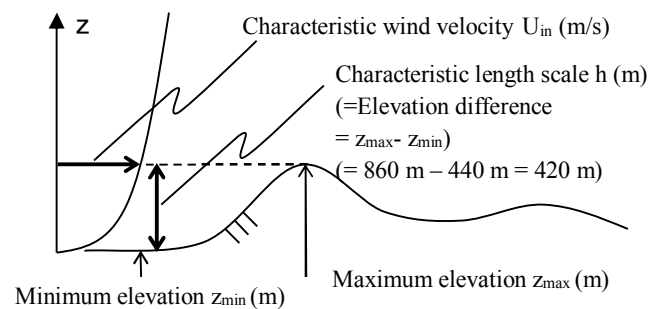

Figure 5. Computational grid cells in the vicinity of the wind turbines
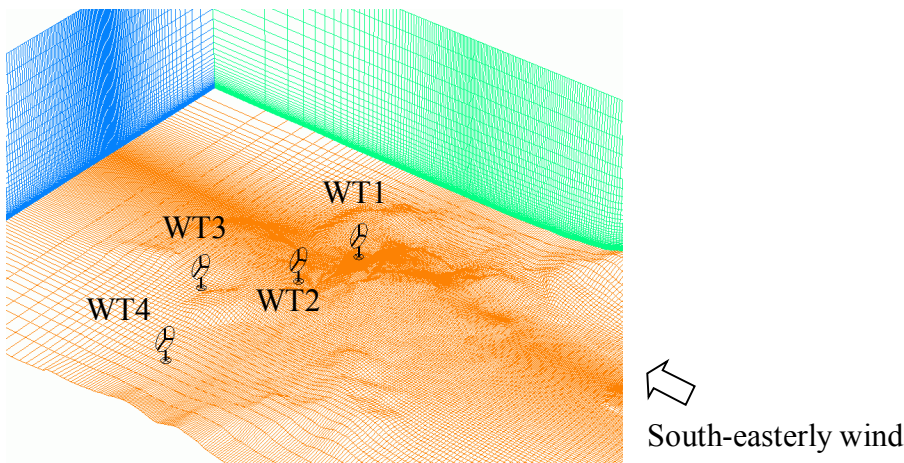
Figure 6. E_{pV} (wind velocity profile) as given in Bulletin No. 1454 of the Ministry of Construction, 2000

Roughness classification	Z_b (m)	Z_G (m)	α
I	5	250	0.10
II	5	350	0.15
III	5	450	0.20
IV	10	550	0.27

Figure 7. Characteristic scales used in the present simulation

3.3. Simulation results and discussions

In the present study, discussions will focus on comparisons between the airflows at WT4, which has had the best operational performance of all the investigated wind turbines, and the airflows at WT2, which is presumed to be affected significantly by terrain-induced turbulence in the case of south-easterly wind. (Wind Turbine 1 - Wind Turbine 4 will be abbreviated as WT1 - WT4 hereafter.)

Fig. 8 shows the wind velocity vectors at the hub height of the wind turbines (78 m above the ground surface). Specifically, the wind velocity vectors are those from the time-averaged wind field. The time interval used for averaging is 100 to 200 in non-dimensional time (see Fig. 10). Fig. 9 shows wind velocity vectors at both of the investigated wind turbine locations from the same time period used for Figs. 8 and 10. The results in Figs. 8 and 9 are equivalent to those that would be found by a RANS time-averaged turbulence model. An examination of both of these results reveals that there exist neither significant wind velocity fluctuations indicating the presence of terrain-induced turbulence nor severe deficits in the wind velocity profiles at the locations of the wind turbines. That is, these results would lead to the conclusion that the wind fields at and around the wind turbines are suitable for wind power generation.

However, breakage has occurred on the yaw motor and yaw gear of WT2. In order to accurately simulate the behavior of terrain-induced turbulence such as that investigated in the present study, the use of the RIAM-COMPACT natural terrain version software, which incorporates an LES model for the unsteady turbulence model, is highly effective. The RIAM-COMPACT software has the ability to output the temporal behaviors of various physical quantities and not just their time-averaged values.

Fig. 10 shows the temporal variation of 1) the fluctuating component (deviation from the mean value) of the streamwise (x) wind velocity at the hub height of the wind turbines and 2) the angle of the wind on horizontal and vertical cross-sections. In the figure, the horizontal axes indicate non-dimensional time. If a wind speed of U_{in} = 5m/s is assumed, the time in the figure corresponds to approximately 40 minutes. Fig. 10 also shows the definitions of the angles of the wind on the horizontal and vertical cross-sections. An inspection of the undulating patterns of the time series in Fig. 10 allows a clear understanding of the change in the unsteady wind conditions occurring near the wind turbines.

Subsequently, the fluctuating component (deviation from the mean value) of the streamwise (x) wind velocity will be examined (top panel in Fig. 10). In contrast to the very small temporal fluctuations of the streamwise wind velocity at WT4, the presence of spike-like temporal fluctuations can be confirmed at WT2. Although it is beyond the scope of the present paper, further examination of temporal wind velocity changes at the lower, upper, left, and right ends of the swept area allows an examination of the moments exerted on the rotor.

An examination of the temporal change of the angle of the wind on the horizontal cross-section (middle panel in Fig. 10) reveals the following: as in the case of the wind velocity, the amplitude of the fluctuations of the angle of the wind on the horizontal cross-section is quite small at WT4. On the other hand, changes in the wind direction exceeding 25º are frequently seen at WT2 (see also Fig. 11). Furthermore, the fact that many spikes occur in the direction of positive values suggests that easterly winds are generated on very short time scales due to the topographic effects.

Figure 8. Wind velocity vectors at the wind turbine hub-height (78 m), time-averaged field. The averaging time period is 100 to 200 in non-dimensional time (see Fig. 10).
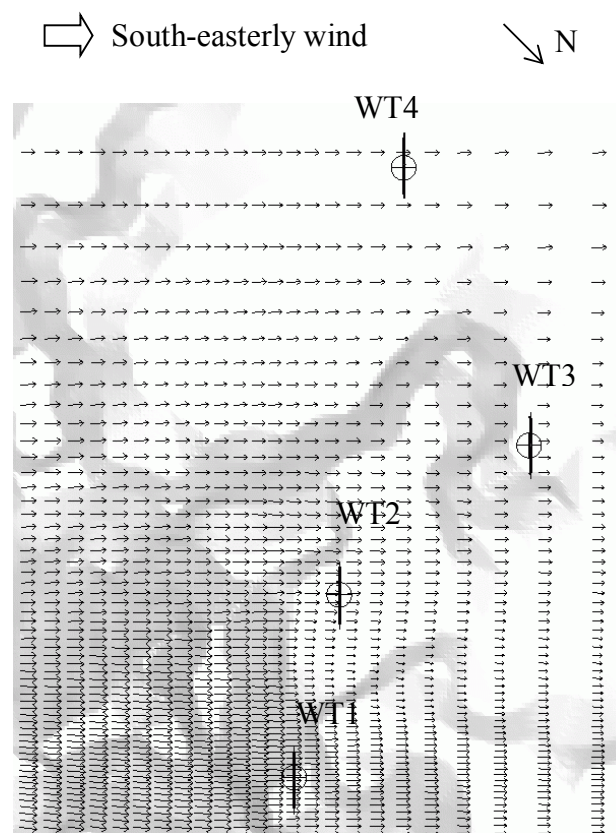
Figure 9. Wind velocity vectors at the wind turbine locations, time-averaged field. The averaging time period is 100 to 200 in non-dimensional time (see Fig. 10).
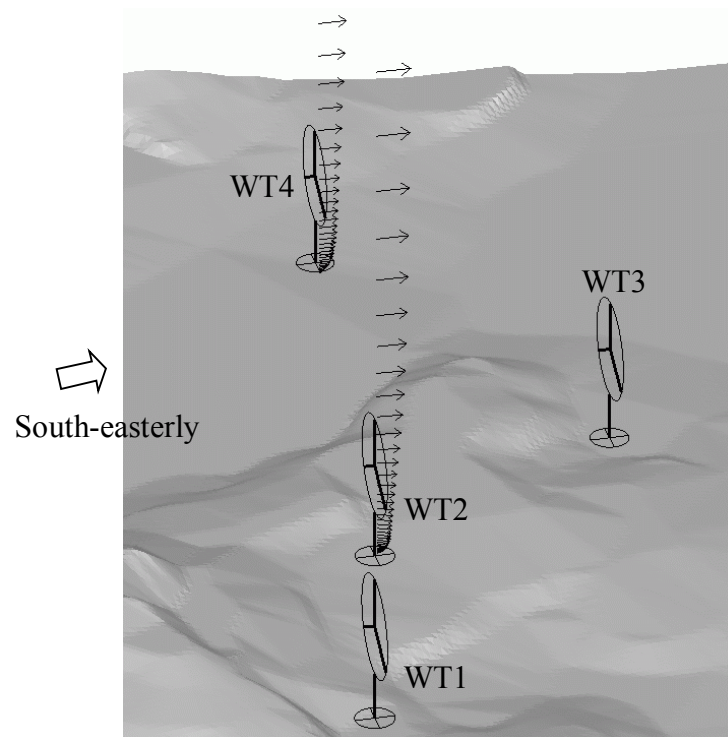
Finally, the temporal change of the angle of the wind on the vertical cross-section is examined (bottom panel in Fig. 10). This figure also suggests that wind blowing upward and downward exceeding 25º from the horizontal is generated. It can be speculated that the minor landforms located upwind of the wind turbine contribute to these local wind direction changes.

Figs. 11 and 12 illustrate the wind field (wind velocity vectors) from times characterized by the large wind direction changes indicated by "A" and "B" in Fig. 10. An examination of Fig. 11 reveals that the direction of the wind aloft at the location of WT2 (easterly wind) deviates significantly from the direction of the prevailing wind. Furthermore, an inspection of Fig. 12, which shows the wind field from a different time from that in Fig. 11, shows that large upward flow has been generated near the center of the hub of WT2. In addition, the vertical profiles of the streamwise wind velocity in Fig. 12 do not follow the so-called wind profile power law; a large velocity deficit can be seen between the hub center and the lower end of the swept area.

In general, the power curve of a wind turbine (the catalog value) is specified using the velocity of the wind flowing into the hub center of the wind turbine on flat terrain assuming the absence of the turbine itself. Furthermore, the vertical profile of the mean horizontal wind speed, which is used to evaluate the wind shear, is assumed to follow a power law with a coefficient of approximately 5 to 7. Therefore, a large reduction in the generated power is expected in the presence of wind shear which deviates significantly from the wind shear predicted using the profile based on the power law. Furthermore, such anomalous wind shear will likely be an increasingly important topic of research in the future in connection with the issues of wind turbine tower vibration and the fatigue strength of yaw gears.

Fig. 13 shows the vertical profiles of selected physical quantities at each of the wind turbine locations. Fig. 13a shows the vertical profile of the mean streamwise wind velocity. Fig. 13b shows the vertical profile of the standard deviation of the streamwise velocity (the horizontal axis indicates the
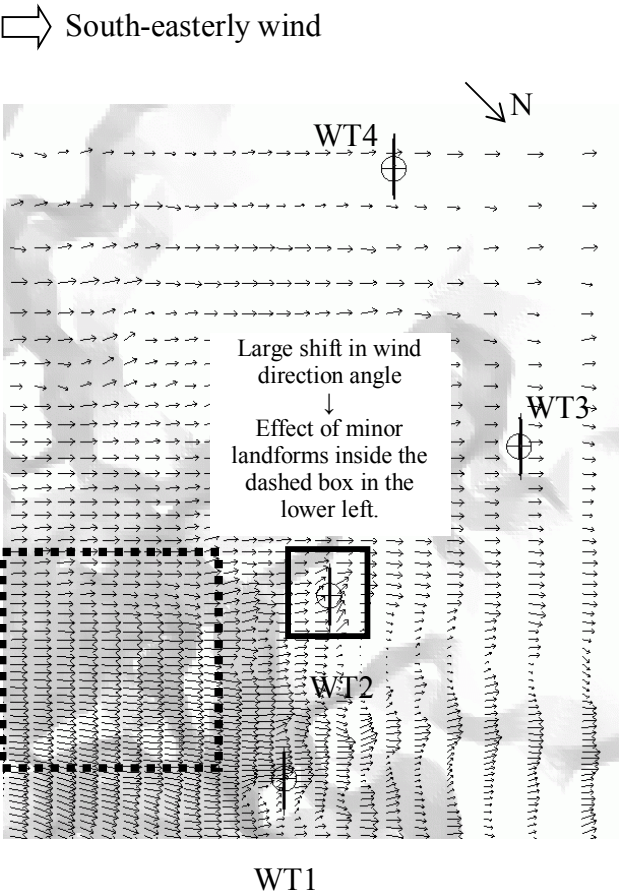
standard derivation normalized by the inflow wind velocity aloft U_{in}). Fig. 13c shows the turbulence intensity (%) evaluated by dividing the standard deviation of the streamwise velocity by the mean streamwise wind velocity $<u>$ at each location. In all these figures, the vertical axes indicate the height above the ground (m). In these figures, the vertical range of the wind turbine swept area (the rotor diameter) is also illustrated. In the vertical profile of the mean streamwise wind velocity in Fig. 13a, no severe wind velocity deficit is identified at any of the wind turbines. An inspection of the profiles in the vertical range of the wind turbines in Figs. 13b and 13c reveals effects of terrain-induced turbulence of a similar magnitude at WT1 and WT3 due to the presence of the minor landforms upstream of these turbines. The effect of the terrain-induced turbulence is notably smaller at WT4 than at the other three wind turbines.

Figure 10. The fluctuating streamwise (x) component of the wind at the hub-height of the wind turbines (top). Temporal change in the angle of the wind on the horizontal (middle) and vertical (bottom) cross-sections. With an assumed wind speed of $U_{in} = 5$m/s, the time period on the horizontal axes is equivalent to approximately 40 minutes.

Definition of the angle on the horizontal cross-section

Definition of the angle on the vertical cross-section
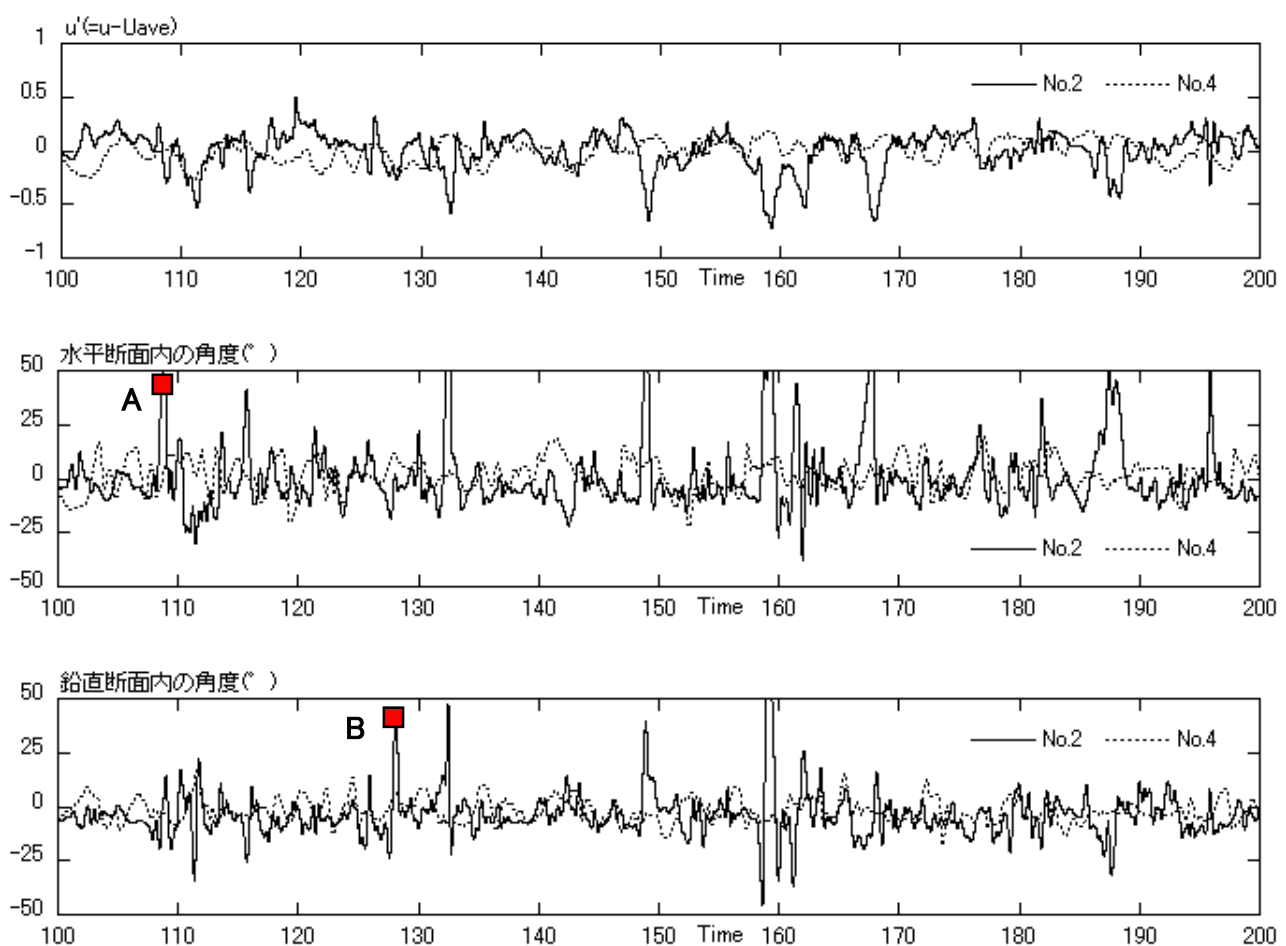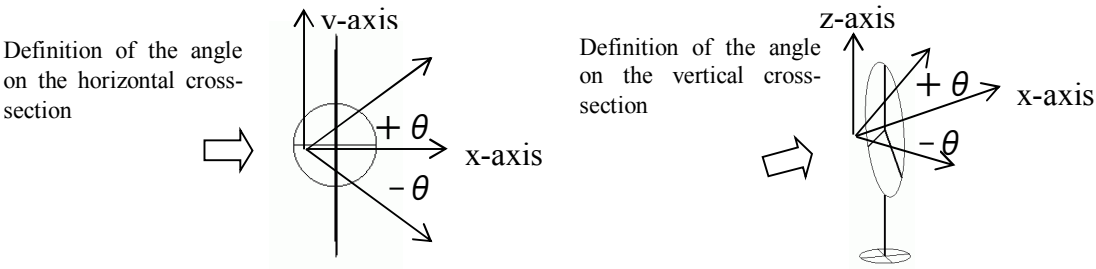
Figure 11. Wind velocity vectors at the wind turbine hub-height (78 m). Instantaneous field from the time indicated by "A" in Fig. 10.

South-easterly wind

WT4

N

Large shift in wind direction angle
↓
Effect of minor landforms inside the dashed box in the lower left.
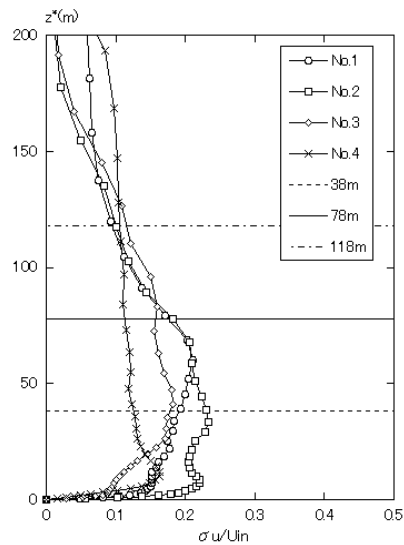
WT3

WT2

WT1

Figure 12. Wind velocity vectors at the wind turbine locations. Instantaneous field from the time indicated by "B" in Fig. 10.
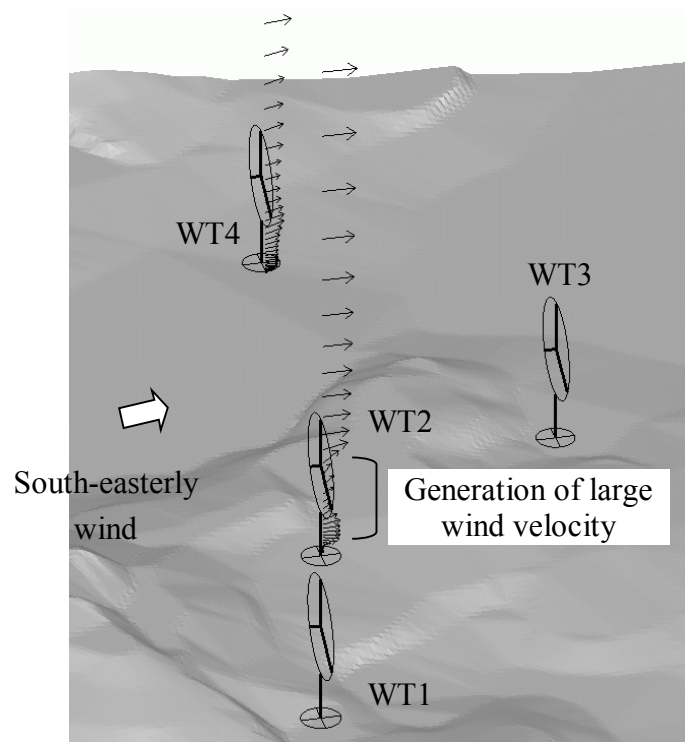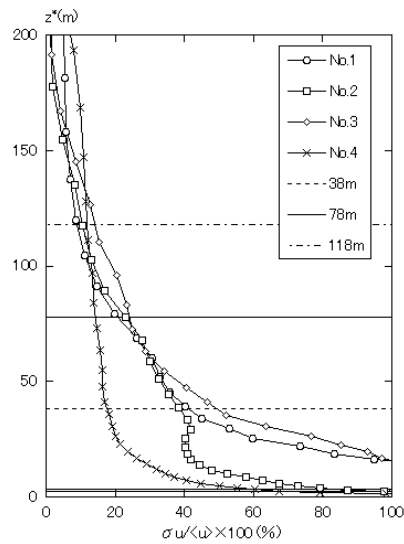

Figure 13. Vertical profiles of various physical quantities at the wind turbine locations
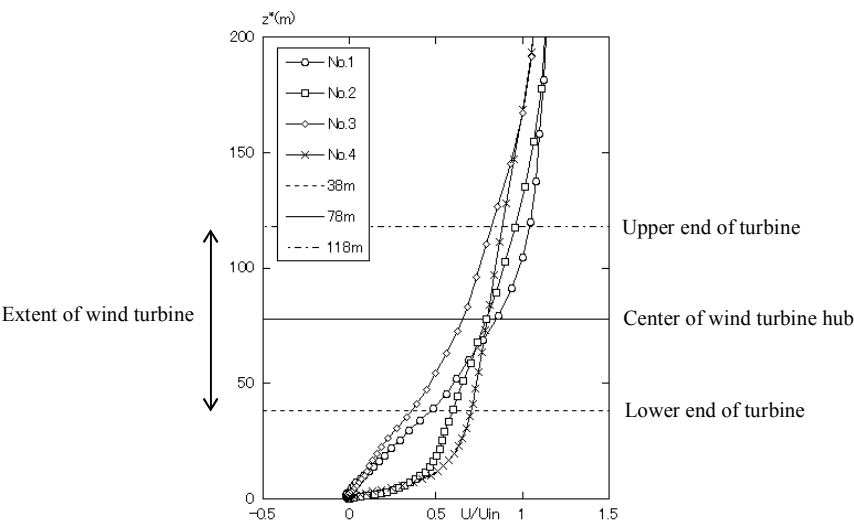
(a) Profiles of mean streamwise wind velocity

(b) Standard deviation of the streamwise wind velocity

(c) Turbulence intensity (%) of the streamwise wind velocity

Figure 14. Trajectories (pathlines) of virtual particles released from the locations of WT2 and WT4. Virtual particles are released at the height of the center of the wind turbine hub, across a straight line between the left and right ends of the swept area.

(a) At non-dimensional time t

(b) At non-dimensional time t + Δt

(c) At non-dimensional time t + 2Δt
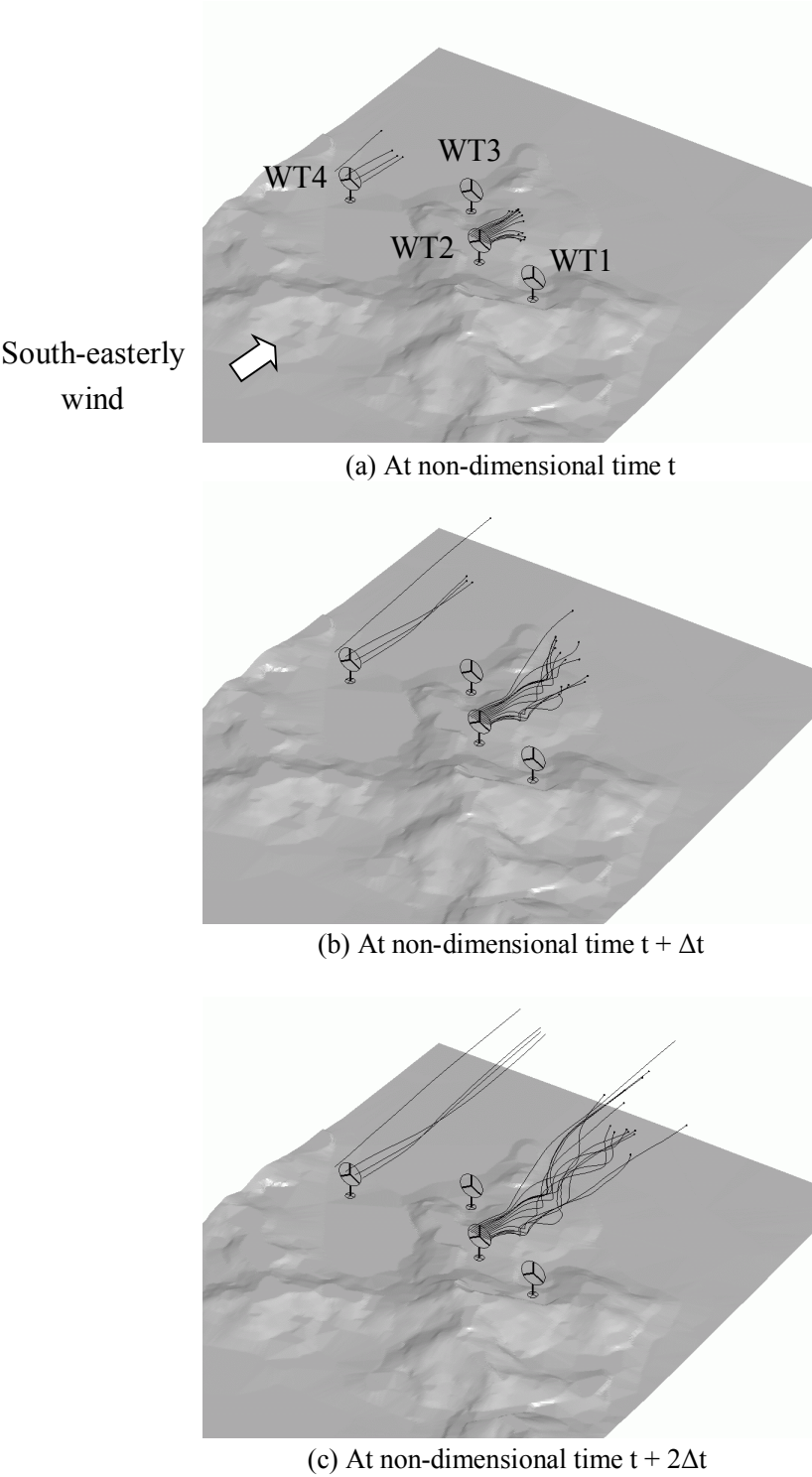
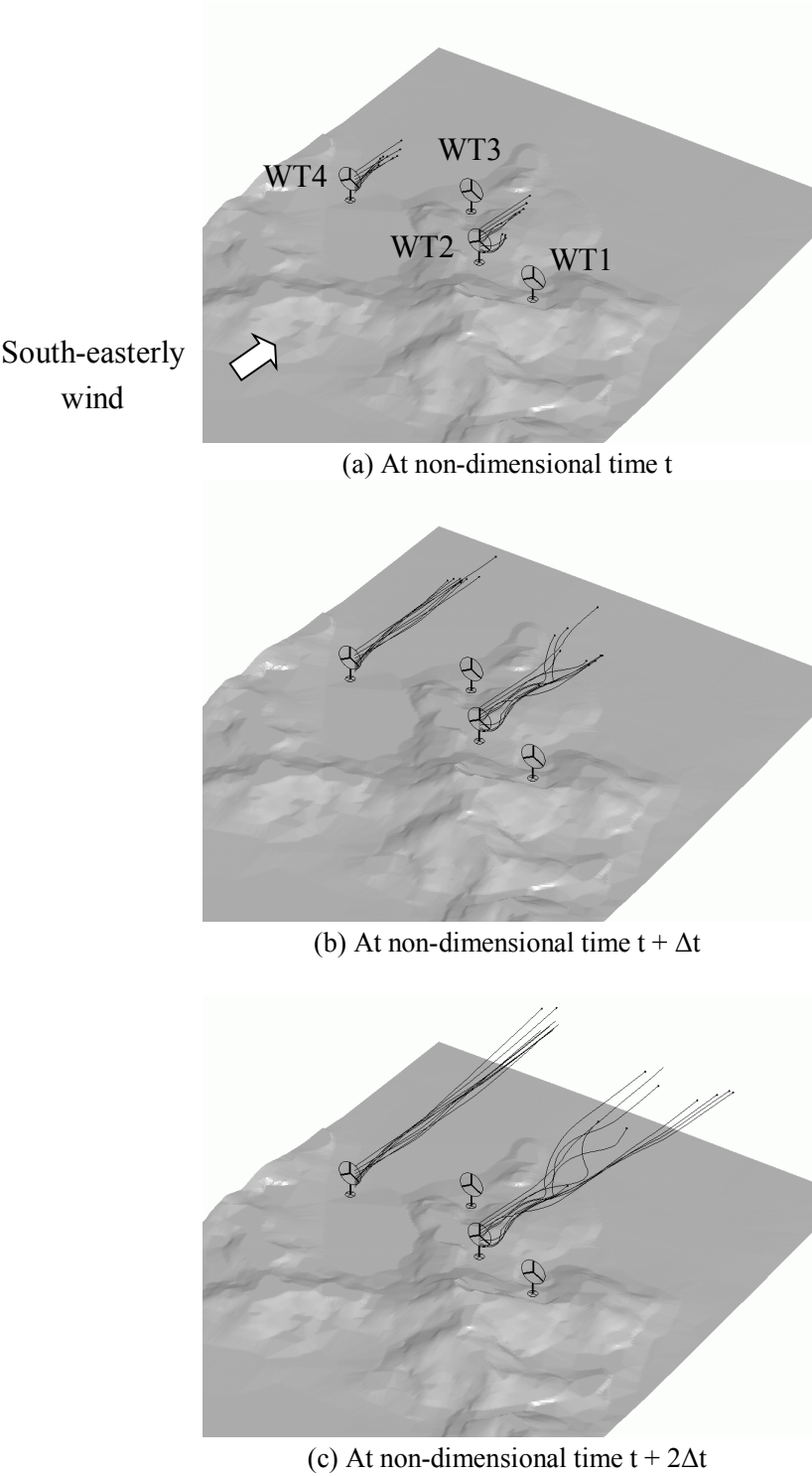**Figure 15.** Trajectories (pathlines) of virtual particles released from the locations of WT2 and WT4. Virtual particles are released at the y-coordinate of the center of the wind turbine hub, across a straight line between the lower and upper ends of the swept area.

(a) At non-dimensional time t

(b) At non-dimensional time t + Δt

(c) At non-dimensional time t + 2Δt

In order to assess three-dimensional wind conditions, it is effective to release virtual particles and observe their trajectories (pathlines). Figs. 14 and 15 show the results obtained using this method. In Fig. 14, virtual particles are released between the right and left edges of the swept area at the height of the center of the wind turbine hub. On the other hand, virtual particles are released between the upper and lower edges of the swept area at the y-coordinate of the center of the wind turbine hub in Fig. 15. As discussed thus far, no major changes of the airflow caused by the terrain exist in the vicinity of WT4, and the particles move smoothly downstream of the wind turbines (Figs. 14 and 15). In contrast, in the vicinity of WT2, the airflow meanders significantly and three dimensionally in the horizontal and vertical directions due to the effects of the minor landforms located upstream of this wind turbine (Figs. 14 and 15).

Finally, it should be recalled that the present study examines only the turbulence generated by the irregularities of the terrain surface and does not take into account the effects of the turbulence caused by gusts.

4. The Economic Effects

At the Atsumi Wind Farm in Aichi Prefecture, Japan (start date of operation: January 17, 2007), damage to wind turbines occurred frequently due to terrain-induced turbulence. The terrain-induced turbulence affected the wind turbines in the form of worn brake pads for yaw motors and fractured planetary gears both due to frequent yaw controls and also in the form of hydraulic system failures due to frequent pitch controls. In the present study, numerical wind diagnoses (analyses of terrain-induced turbulence) were conducted by reproducing the topography in the vicinity of the wind turbine sites in high resolution and using RIAM-COMPACT natural terrain version, which is based on large eddy simulation (LES). The results of the diagnoses indicated that, in the case of south-easterly wind, terrain-induced turbulence is generated at a small terrain feature located upstream of Wind Turbine (WT) #2, which serves as the origin of the turbulence. The generated turbulence strongly affects the wind turbine, causing the wind speed and direction at the wind turbine site to change significantly with time. At the Atsumi Wind Farm, a combination of the series of wind diagnoses and on-site operation experience led to a decision to adopt an "automatic shutdown program" for WTs #1 and #2 (introduced on May 23, 2011; modified on July 26, 2011). Here, "automatic shutdown program" refers to the automatic suspension of wind turbine operation upon the wind speed and direction meeting the conditions associated with significant effects of terrain-induced turbulence at a wind turbine site. Specifically, after modifications, the program was configured such that WT #1 would stop operation for the wind direction range of 130 to 190º with wind speeds of 9 m/s or higher and that WT #2 would stop operation for the wind direction range of 90 to 130º with wind speeds of 10 m/s or higher. The adoption of the "automatic shutdown program" has successfully resulted in a large reduction in the number of occurrences of wind turbine damage, thus, creating major positive economic effects. To evaluate the economic effects, the performance of the wind turbines from the two years preceding the adoption of the "automatic shutdown program" was used as a reference, and changes in the capacity and availability factors were calculated from the reduction in downtime of the wind turbines from the two years following the adoption of the "automatic shutdown program." The following economic effects have been realized based on converting the performance of the two wind turbines combined from the two years preceding and the two years following the adoption of the "automatic shutdown program" into the performance of a single wind turbine per year: 1) a reduction in the repair costs by 9.322 million yen per year per wind turbine, 2) an increase in the availability factor by 8.05% (87.3% → 95.4%), and 3) an increase in the capacity factor by 1.7% (21.2% → 22.9%). The number of

occurrences of damage to wind turbines can be reduced significantly by combining suitability inspections of local wind conditions" by RIAM-COMPACT, that is, numerical wind diagnoses (analyses of terrain-induced turbulence), with appropriate wind turbine control based on the results of the diagnoses. At the same time, this combination of approaches also results in significant positive economic effects. In the future development of the wind power industry in Japan, it is essential to adopt suitability inspections of local wind conditions" for each of the country's land-based wind turbines.

5. Conclusions

The wind conditions at the Atsumi Wind Farm in Aichi Prefecture, Japan (in operation since March 2007) were numerically predicted using the RIAM-COMPACT natural terrain version software. The simulation results showed that the minor landforms located upstream of WT2 serve as the origin of turbulence (terrain-induced turbulence) in the case of south-easterly wind and that WT2 is strongly affected by this turbulence.

The use of time-averaged RANS turbulence models creates severe difficulties in simulating the effects of terrain-induced turbulence generated locally due to minor landforms and small topographical irregularities distributed sparsely around wind turbines. As a result, the use of RANS models tends to miss the presence of such effects. Therefore, it is effective to adopt an approach based on an unsteady turbulence model (e.g., LES) such as RIAM-COMPACT.

In addition, relative comparisons of the effects of terrain-induced turbulence among wind turbines as that presented in the present study can be made appropriately using only detailed terrain data accurately representing the land formations at a site of interest, without the use of any meteorological data. If the results from such comparisons were to be effectively applied to wind turbine operation control, the number of internal and external breakdowns of WTGs caused by terrain-induced turbulence would decrease dramatically, which would likely allow the availability factors of wind turbines to increase significantly. For example, meteorological conditions in which large wind direction and speed changes occur so rapidly that they cannot be adequately counteracted by the pitch angle control of the wind turbine blades (i.e., specific wind directions in which such meteorological conditions occur) can be predicted in advance for the position of each nacelle. When the actual meteorological conditions meet the previously identified meteorological conditions, measures such as halting wind power generation can be taken (see Fig. 16).

Figure 16. Conceptual diagram of operation control
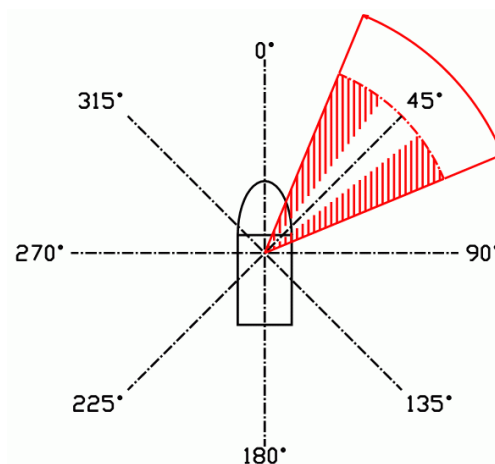
Wind direction range for which operation control is applied

Wind directions in which large wind direction and speed fluctuations occur due to topographical effects.

In the future, regardless of whether the terrain is flat or complex, it is necessary 1) to conduct a detailed wind synopsis diagnosis as the one presented in this paper for all wind directions around a wind turbine and 2) to accurately understand the three-dimensional local wind conditions at each wind turbine location the temporal change of the vertical profiles of the wind velocities at wind turbine locations and 2) wave-like structures in the time series of the wind velocities and the turbulence intensities at the lower, upper, left, and right ends of the swept area.

References

1) J. Berg, J. Mann, A. Bechmann, M. S. Courtney, and H. E. Jørgensen, The Bolund experiment, part I: flow over a steep, three-dimensional hill, Boundary-Layer Meteorology, vol. 141, no. 2, pp. 219–243, 2011

2) A. Bechmann, N. N. Sørensen, J. Berg, J. Mann, and P.-E. Réthoré, The Bolund experiment, part II: blind comparison of microscale flow models, Boundary-Layer Meteorology, vol. 141, no. 2, pp. 245–271, 2011

3) J. M. Prospathopoulos, E. S. Politis, and P. K. Chaviaropoulos, Application of a 3D RANS solver on the complex hill of Bolund and assessment of the wind flow predictions, Journal of Wind Engineering and Industrial Aerodynamics, vol. 107-108, pp. 149–159, 2012

4) M. Diebold, C. Higgins, J. Fang, A. Bechmann, and M. B. Parlange, Flow over hills: a large-eddy simulation of the Bolund case, Boundary-Layer Meteorology, vol. 148, no. 1, pp. 177–194, 2013

5) T. S. Yeow, A. Cuerva, B. Conan, and J. Pérez-Álvarez, Wind tunnel analysis of the detachment bubble on Bolund Island, Journal of Physics: Conference Series, vol. 555, no. 1, Article ID 012021, 2014

6) T. S. Yeow, A. Cuerva-Tejero, and J. Pérez-Álvarez, Reproducing the Bolund experiment in wind tunnel, Wind Energy, vol. 18, no. 1, pp. 153–169, 2015

7) Ashvinkumar Chaudhari, Antti Hellsten,and Jari Hämäläinen, Full-Scale Experimental Validation of Large-Eddy Simulation of Wind Flows over Complex Terrain: The Bolund Hill, Advances in Meteorology, Volume 2016, 2016

8) B. Conan, A. Chaudhari, S. Aubrun, J. van Beeck, J. Hämäläinen, and A. Hellsten, Experimental and numerical modelling of flow over complex terrain: the Bolund hill, Boundary-Layer Meteorology, vol. 158, no. 2, pp. 183–208, 2016

9) Takanori Uchida and Yuji Ohya, Verification of the Prediction Accuracy of Annual Energy Output at Noma Wind Park by the Non-Stationary and Non-Linear Wind Synopsis Simulator, RIAM-COMPACT, Journal of Fluid Science and Technology, Vol.3, No.3, pp.344-358, 2008

10) Takanori Uchida and Yuji Ohya, Latest Developments in Numerical Wind Synopsis Prediction Using the RIAM-COMPACT CFD Model-Design Wind Speed Evaluation and Wind Risk (Terrain-Induced Turbulence) Diagnostics in Japan, Energies, Vol.4, pp.458-474, 2011

11) Fumihito Watanabe and Takanori Uchida, Micro-siting of Wind Turbine in Complex Terrain : Simplified Fatigue Life Prediction of Main Bearing in Direct Drive Wind Turbines, WIND ENGINEERING, 39, 4, 21, pp.349-368, 2015

12) Takanori UCHIDA，High-Resolution LES of Terrain-Induced Turbulence around Wind Turbine Generators by Using Turbulent Inflow Boundary Conditions，Open Journal of Fluid Dynamics, Vol.7, pp.511-524, 2017

13) Takanori UCHIDA，High-Resolution Micro-Siting Technique for Large Scale Wind Farm Outside of Japan Using LES Turbulence Model, Energy and Power Engineering, Vol.09, pp.802-813, 2017

14) Takanori UCHIDA，CFD Prediction of the Airflow at a Large-Scale Wind Farm above a Steep,Three-Dimensional Escarpment, Energy and Power Engineering, Vol.09, pp.829-842, 2017

15) Yasushi KAWASHIMA and Takanori UCHIDA, Effects of Terrain-Induced Turbulence on Wind Turbine Blade Fatigue Loads, Energy and Power Engineering, Vol.9, pp.843-857, 2017

16) Takanori UCHIDA，Large-Eddy Simulation and Wind Tunnel Experiment of Airflow over Bolund Hill, Open Journal of Fluid Dynamics, Vol.8, pp.30-43, 2018

17) Kim, J. and Moin, P., Application of a fractional-step method to incompressible Navier-Stokes equations, J. Comput. Phys., Vol.59 (1985), pp.308-323

18) Kajishima, T., Upstream-shifted interpolation method for numerical simulation of incompressible flows, Bull. Japan Soc. Mec. Eng. B, 60-578 (1994), pp.3319-3326, (in Japanese)

19) Kawamura, T., Takami, H. and Kuwahara, K., Computation of high Reynolds number flow around a circular cylinder with surface roughness, Fluid Dyn. Res., Vol.1 (1986), pp.145-162

20) Smagorinsky, J., General circulation experiments with the primitive equations, Part 1, Basic experiments, Mon. Weather Rev., Vol.91 (1963), pp.99-164